Load Modulated Balanced Amplifier Design Method Based on Complex Impedance Trajectories

Kimon Vivien, Paolo Enrico de Falco, Olivier Venard, Geneviève Baudoin, Pascal Pierre-Charles-Felix, Taylor Barton

IEEE Journal of Microwaves

Received 27 September 2021; revised 8 November 2021; accepted 9 November 2021. Date of publication 23 December 2021; date of current version 7 January 2022.

Digital Object Identifier 10.1109/JMW.2021.3129168

Load Modulated Balanced Amplifier Design Method Based on Complex Impedance Trajectories

KIMON VIVIEN [1] (Member, IEEE), PAOLO ENRICO DE FALCO [2] (Member, IEEE), OLIVIER VENARD [1], GENEVIÈVE BAUDOIN [1], PASCAL PIERRE-CHARLES-FÉLIX [3], AND TAYLOR BARTON [2] (Senior Member, IEEE)

(Regular Paper)

[1]System Engineering Department, ESIEE Paris, ESYCOM FRE2028, Université Paris-Est, 77420 Noisy-le-Grand, France
[2]Department of Electrical, Computer, and Energy Engineering, University of Colorado Boulder, Boulder, CO 80309 USA
[3]SOMOS Semi-Conductor, 78160 Marly-le-Roi, France

CORRESPONDING AUTHOR: Taylor Barton (e-mail: taylor.w.barton@colorado.edu).

This work was supported by the Office of Naval Research (ONR) under Award N00014-21-1-2465, monitored by Dr. Paul Maki.

ABSTRACT This paper presents a design methodology for a load modulated balanced amplifier (LMBA) focusing on AMPM distortion mitigation. By introducing second harmonic control as a degree of design freedom, a complex load trajectory can be selected to compensate for AMPM nonlinearities in the device without substantially affecting efficiency. A mathematical derivation is accompanied by a design procedure based on closed-form equations to fabricate an LMBA based solely on load-pull data. The theory is validated through the measured comparison of three different designs operating at 2.4 GHz in a pseudo-RF-input Doherty-like LMBA configuration, with class-J, -B, and -J* main PAs. The class-J prototype outperforms the other designs with 54% and 49% drain efficiency at peak output power and 6-dB back-off, respectively, and only 4 degrees of AM-PM across this power range. When driven with a 10-MHz, 8.6-dB PAPR LTE signal, 40.5% average efficiency is achieved with better than −40.5 dBc ACLR without digital predistortion.

INDEX TERMS Class J, Doherty power amplifier, gallium nitride, load modulated balanced amplifier, power amplifiers.

I. INTRODUCTION

Modern communication standards emphasize high spectral efficiency, leading to signals with high peak-to-average power ratios (PAPRs). These signals require power amplifiers (PAs) that are not only efficient over a wide output power dynamic range, but that introduce low distortion in response to widely-varying signal amplitudes. Although digital predistortion (DPD) can be used to mitigate nonlinear effects, it is often desirable to limit the complexity of the DPD, particularly in low-power applications where power consumption of the DPD is not negligible [1], or in arrays where element-level DPD is not easily implemented [2]. It is therefore of interest to develop PA architectures able to favorably trade off efficiency and linearity through a straightforward design method.

Efficiency enhancement can be achieved by dynamically modulating the impedance seen by a transistor, as in the Doherty PA (DPA) [3]–[12] or outphasing PA [13]–[17]. Load modulation PA architectures are typically composed of two or more transistors that interact through a non-isolating power combining network. Through asymmetric operation in amplitude and/or phase, each device controls the impedance seen by the other, thereby tracing a load trajectory that maintains efficiency while modulating the output power.

A promising architecture employing load modulation is the recently developed load modulated balanced amplifier (LMBA) [18]–[29]. As shown in Fig. 1, active load modulation is achieved in the LMBA by injecting a current into the isolated port of a balanced amplifier through a control PA. In [22], an RF-input Doherty-like LMBA is presented in which the balanced and control transistors are biased in class B and C respectively and the injected "control" signal is generated from the single RF input through an input power division. The resulting PA performs on par with state-of-the-art DPAs but with a more favorable device scaling ratio between the

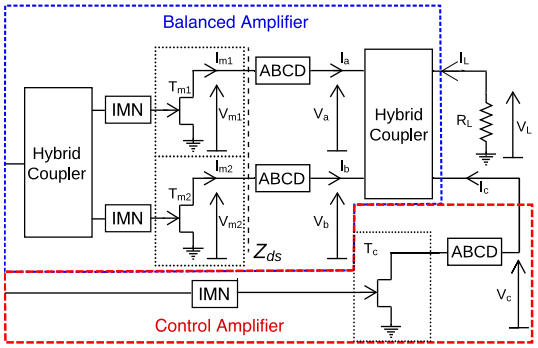

FIGURE 1. Simplified schematic of the LMBA as used for the theoretical analysis.

main and control transistors. Variations on the LMBA architecture have been explored [25], [30], with the majority of the literature focusing on back-off efficiency enhancement and bandwidth. One approach [29], [31] inverts the biasing approach of the Doherty-like LMBA so that the control PA is biased in class B. This technique has been shown to theoretically implement a flat AMAM characteristic [29], but AMPM effects have not been explored. This critical contributor to PA distortion is the focus of this work.

Because both the gain and phase response of a transistor are strongly dependent on the impedance presented to the drain [32], load modulated amplifiers are subject to amplitude and phase distortions that are a combination of the intrinsic transistor behavior due to input amplitude variation, i.e., conventional AMAM and AMPM effects, and distortion caused by load modulation. In the region of active load modulation, these load-to-amplitude (LMAM) and load-to-phase (LMPM) nonlinearities are due to the Miller effect, with the LMPM the dominating generator of phase distortion [6], [33]. A circuit-design based solution to improve phase distortion in load-modulated PAs is to select the impedance trajectories so as to compensate for the transistors' AMPM response. This approach is employed for example in [6] by using complex impedance trajectories in a DPA to reach a linearity-efficiency compromise. A drawback of the DPA application, however, is that the load trajectory of the main and auxiliary PAs are interdependent through the combining network design.

When a complex impedance trajectory is employed at the fundamental frequency, it is important to also consider the effects of harmonic impedance termination. The second harmonic impedance in particular has been related to a fixed, complex fundamental impedance to describe the class B-J continuous classes [34]. Appropriate selection of harmonic terminations has been long established as a way to improve PAE [35], [36] or linearity [37] in PAs driving a fixed load. While the selection of harmonic termination is not explicitly considered in [6] as a design tool, there is opportunity for using harmonic waveform shaping to similarly enhance performance within a load-modulated architecture [16].

In this work, we explore the Doherty-like LMBA architecture as a vehicle for AMPM distortion reduction. The approach exploits the LMBA architecture's ability to present an arbitrary load trajectory to the load-modulated main PA independent of the control PA's operation. Through a combination of harmonic waveform shaping and fundamental load impedance trajectory selection, a design procedure is presented that is able to favorably trade off linearity and efficiency.

Our related conference paper [28] presented an initial measurement of a class-J LMBA demonstrating a linearity-efficiency tradeoff of two different complex trajectories using a fixed phase offset. Likewise in [38] a linearity dependence on the relative phase offset in a dual-input LMBA drive is demonstrated, although the fundamental cause is not analyzed. Here, we derive the theoretical effects of impedance and introduce a complete design methodology including effects of the second harmonic. We present closed-form equations describing the phase and amplitude response of the LMBA as determined by the impedances presented at maximum output power and output back-off (OBO). By applying this analysis to simulated load-pull information from a single-ended transistor, the combined linearity and efficiency of the LMBA is predicted. To validate the theory in measurement, three PAs are designed with equal peak output power but with class J, B, and J* harmonic terminations. We show that in the case of the class-J LMBA, the reactively terminated second harmonic naturally corresponds to a complex impedance trajectory that minimizes AMPM distortion during load modulation, while keeping high efficiency. Furthermore, the efficiency-linearity tradeoff can be adjusted after fabrication through pseudo RF-input operation, a possibility not available in the DPA.

Section II presents a derivation predicting the LMBA distortion characteristics based on the generalized architecture. Section III describes the impact of the load trajectory on LMBA performance, and specifically AMAM and AMPM distortion. A design methodology for developing a linear and efficient LMBA from load-pull data is presented in Section IV. Section V presents details of the three example 2.4-GHz designs. Measured characterization, including both continuous wave (CW) and modulated signals, are given in Section VI. Section VII concludes the paper.

II. GENERALIZED LMBA ANALYSIS

Fig. 1 shows a generalized LMBA schematic, consisting of the main balanced PA having two hybrid couplers and main transistors T_{m_1} and T_{m_2}, and the control PA based on transistor T_c. We note here the following nomenclature: the subscripts *m1*, *m2*, *c* and *L* refer to the two branch transistors, control transistor and output port respectively. The subscripts bo and max describe the values of the different voltages/currents at back-off ($\beta = \beta_{\text{bo}}$) and at peak power ($\beta = 1$). Whereas previous works have followed an analysis in terms of the back-off design parameter γ [22], here we focus on the impedances selected at peak (Z_{max}) and back-off (Z_{bo}) power levels. This impedance-based analysis will be the basis of the load impedance trajectory design methodology.

In the Doherty-like LMBA approach employed in this work, the control PA is turned on in the high-power region to generate load modulation [20], [22]. We can distinguish two operating regions, depending on the input drive level, β:

- Back-off, $0 < \beta < \beta_{\text{bo}}$: the control amplifier is off. The main transistors see a fixed load impedance Z_{bo} and will saturate at an input drive level $\beta = \beta_{\text{bo}}$, called the break-point. The current I_c is zero while $I_{m_{1,2}}$ scale linearly with β. To achieve high efficiency at the break-point, the in-phase component of the drain voltages $V_{m_{1,2}}$ must reach their maximum swing value $V_{\max}$.
- Load modulation, $\beta_{\text{bo}} < \beta < 1$: the control amplifier turns on and starts modulating the main transistors' load impedance. Both the main and the control amplifier will saturate at the input drive level $\beta = 1$ and $|I_{m_{1,2}}| = I_{\max}/2$, the maximum fundamental drain current. I_c is related to $I_{m_{1,2}}$ by a current factor $\alpha e^{-j\phi}$. At $\beta = 1$, the in-phase component of the voltages $V_{m_{1,2}}$ must once again be equal to $V_{\max}$ for high efficiency.

A. LMBA OPERATION

The generalized LMBA operation has been derived in various other works [18]–[22] for ideal systems and is briefly summarized here. In order to explicitly operate at the intrinsic drain of the device, the ABCD parameter blocks in Fig. 1 representing the generalized output matching networks (OMNs) and transistor parasitics (mainly C_{ds}) are first considered. In back-off, when the control amplifier is off and there is thus no load modulation, the OMN of the balanced amplifiers must match Z_0 to a fixed desired impedance $Z_{\text{bo}} = R_{\text{bo}} + jX_{\text{bo}}$. The OMNs are assumed to have been appropriately designed to perform this impedance match with some arbitrary phase shift θ_{OMN}. Then, following the generalized LMBA analysis in [20], [22] and the approach in [39], the impedance presented at the main transistors' drains can be expressed as:

$$Z_{m_{1,2}} = Z_{\text{bo}}\left(1 - j\sqrt{2}\frac{\sqrt{R_{\text{bo}}Z_0}e^{-j\theta_{\text{OMN}}}}{Z_{\text{bo}}}\frac{I_c}{I_{m_1}}\right) \tag{1}$$

The voltages at the remaining ports of the hybrid coupler are

$$V_L = -Z_0\left(\sqrt{\frac{2R_{\text{bo}}}{Z_0}}e^{-j\theta_{\text{OMN}}} - j\frac{I_c}{I_{m_1}}e^{-2j\theta_{\text{OMN}}}\right)I_{m_1} \tag{2}$$

and

$$V_c = I_c Z_0 \tag{3}$$

Equations (1), (2), and (3) capture the fundamental operation of the LMBA. By separately controlling the currents I_{m_1} and I_c, the impedance seen by each main transistor can be changed, while the control amplifier is isolated and drives a fixed load. As opposed to the DPA, the load modulation is only dependent on the current ratios, and is not constrained through the combiner design. The modulated load can therefore take any value on the Smith chart.

B. DOHERTY-LIKE LMBA

We next apply a Doherty-like input drive scheme to the generalized LMBA equations. In order to establish current continuity between the back-off and load-modulation operating regimes as described above, at the break-point β_{bo} we can write the following expressions for the currents:

$$\begin{aligned} I_{m1}|_{\beta=\beta_{\text{bo}}} &= \beta_{\text{bo}}\frac{I_{\max}}{2}e^{-j\Theta_{\beta_{\text{bo}}}} \\ I_{m2}|_{\beta=\beta_{\text{bo}}} &= -j\beta_{\text{bo}}\frac{I_{\max}}{2}e^{-j\Theta_{\beta_{\text{bo}}}} \\ I_c|_{\beta=\beta_{\text{bo}}} &= 0 \end{aligned} \tag{4}$$

At peak drive when $\beta = 1$:

$$\begin{aligned} I_{m1}|_{\beta=1} &= \frac{I_{\max}}{2} \\ I_{m2}|_{\beta=1} &= -j\frac{I_{\max}}{2} \\ I_c|_{\beta=1} &= \alpha e^{-j\phi}\frac{I_{\max}}{2} \end{aligned} \tag{5}$$

With the phase of the current I_{m1} at maximum drive defined as the reference (zero) point, the currents I_{m1} and I_{m2} have in back-off a phase offset represented as $\Theta_{\beta_{\text{bo}}}$. This factor, which we term the LMPM, describes the phase variation of the intrinsic drain current due to the change of the operating point (both load impedance and input power) between the peak power and back-off power conditions. This characteristic relates to the Miller effect and is dependent on the device technology. It is the source of the very high phase distortion in load modulated amplifiers, with typical values in the range of 10 to 30 degrees for GaN devices [33]. Because $\Theta_{\beta_{\text{bo}}}$ depends on the nonlinear behaviors intrinsic to the device, we do not attempt to model it but will instead determine its behavior through large-signal load-pull simulation in the next section.

Requiring maximum efficiency at both back-off and maximum power results in the second boundary condition. Maximum efficiency is obtained when the in-phase component of the drain voltage reaches the dc supply voltage. Equating these two voltages results in the following relationship between β_{bo} and the impedances $Z_{m_{1,2}}$ at these two power points:

$$\begin{aligned} \text{Re}\left\{\frac{\text{I}_{\max}}{2}\beta_{\text{bo}}\text{Z}_{\text{m}_{1,2}}|_{\beta=\beta_0}\right\} &= \text{Re}\left\{\frac{\text{I}_{\max}}{2}\text{Z}_{\text{m}_{1,2}}|_{\beta=1}\right\} \\ \beta_{\text{bo}} &= \frac{\text{Re}\left\{\text{Z}_{\text{m}_{1,2}}|_{\beta=1}\right\}}{\text{Re}\left\{\text{Z}_{\text{m}_{1,2}}|_{\beta=\beta_0}\right\}} \end{aligned} \tag{6}$$

Applying these boundary equations to the current I_L and the impedances seen by the main transistors yields:

$$Z_{m_{1,2}}|_{\beta=\beta_0} = Z_{\text{bo}} \tag{7}$$

$$Z_{m_{1,2}}|_{\beta=1} = Z_{\text{bo}} - j\sqrt{2}\alpha e^{-j\phi}\sqrt{R_{\text{bo}}Z_0}e^{-j\theta_{\text{OMN}}} \tag{8}$$

$$I_{L_{\text{bo}}} = \frac{I_{\max}}{2}e^{-j\Theta_{\beta_{\text{bo}}}}\sqrt{\frac{2R_{\text{bo}}}{Z_0}}\frac{\text{Re}\left\{\text{Z}_{\text{m}_{1,2}}|_{\beta=1}\right\}}{\text{Re}\left\{\text{Z}_{\text{m}_{1,2}}|_{\beta=\beta_0}\right\}}e^{-j\theta_{\text{OMN}}} \tag{9}$$

$$I_{L_M} = \frac{I_{\max}}{2}\left(\sqrt{\frac{2R_{\text{bo}}}{Z_0}} - j\alpha e^{-j\phi}e^{-j\theta_{\text{OMN}}}\right)e^{-j\theta_{\text{OMN}}} \quad (10)$$

Finally, considering (9) and writing the impedance presented at maximum output power as $Z_{m_{1,2}}|_{\beta=1} = Z_{\max}$, with $Z_{\max} = R_{\max} + jX_{\max}$, we can define the current factor $\alpha e^{-j\phi}$ in terms of $Z_{\max}$ and Z_{bo} as:

$$\alpha e^{-j\phi} = j\frac{Z_{\max} - Z_{\text{bo}}}{\sqrt{2R_{\text{bo}}Z_0}}e^{j\theta_{\text{OMN}}} \quad (11)$$

We can now express the load current I_L at back-off and peak power conditions based on the expected peak and back-off load impedances and the maximum current $I_{\max}$:

$$I_{L_{\text{bo}}} = \frac{R_{\max}}{R_{\text{bo}}}\sqrt{2\frac{R_{\text{bo}}}{Z_0}}e^{-j\theta_{\text{OMN}}}\frac{I_{\max}}{2}e^{-j\Theta_{\text{bo}}}$$

$$I_{L_{\max}} = \frac{Z_{\max} + Z_{\text{bo}}^*}{\sqrt{2R_{\text{bo}}Z_0}}e^{-j\theta_{\text{OMN}}}\frac{I_{\max}}{2} \quad (12)$$

From (12) we can identify some key parameters of the LMBA. The output back-off and maximum power levels can be related to the maximum power of each branch transistor and the load trajectory:

$$P_{L_{\max}} = P_{m_{max}}\frac{|Z_{\max} + Z_{\text{bo}}^*|^2}{2R_{\text{bo}}R_{\max}}$$

$$P_{L_{\text{bo}}} = 2P_{m_{\max}}\frac{R_{\max}}{R_{\text{bo}}} \quad (13)$$

where $P_{m_{\max}}$ is the maximum power of the transistors $T_{m_{1,2}}$.

The dynamic range (or back-off range) γ, describing the relative output power between the back-off and maximum drive level is written as

$$\gamma = \frac{P_{L_{\max}}}{P_{L_{\text{bo}}}} = \left|\frac{Z_{\max} + Z_{\text{bo}}^*}{2R_{\max}}\right|^2 \quad (14)$$

We define the LMBA amplitude distortion (AMAM) as the ratio of the gain of the LMBA at back-off and peak power. Similarly, the total phase distortion (AMPM) of the LMBA is described as the ratio of the phase of the output voltage V_L at the same power levels:

$$\text{AMAM} = \frac{P_{L_{\max}}/P_{in_{\max}}}{P_{L_{\text{bo}}}/P_{in_{\text{bo}}}} = \frac{|Z_{\max} + Z_{\text{bo}}^*|^2}{4R_{\text{bo}}R_{\max}}\frac{G_{m1_{\max}}}{G_{m1_{\text{bo}}}} \quad (15)$$

$$\text{AMPM} = \angle(\Delta V_L) = \angle(Z_{\max} + Z_{\text{bo}}^*) - \Theta_{\text{bo}} \quad (16)$$

Here, $G_{m1_{\max}}$ and $G_{m1_{\text{bo}}}$ correspond to the gain of the branch amplifiers at maximum and back-off power levels and Θ_{bo} is the previously defined load-dependent phase factor of the intrinsic drain current (LMPM) of the branch amplifiers.

As can be seen, the amplitude and phase nonlinearity of the LMBA depends on both the transistor behavior ($G_{m1_{\max}}$, $G_{m1_{\text{bo}}}$, Θ_{bo}) and the selected load trajectory ($Z_{\max}$, Z_{bo}). Therefore, if the transistor's characteristics for different impedances are well known, the impedance trajectory can be selected to influence the linearity in the LMBA architecture. Furthermore, unlike in the Doherty architecture where the load trajectory is designed into the combiner structure, the flexibility of the LMBA load-modulation operation allows for trajectory selection to be designed into the input signal separation (either in hardware or in a dual-input mode) after fabrication and characterization of the output stage.

C. CONTROL AMPLIFIER ANALYSIS

The control PA drives a fixed load, as seen from (3), and can therefore be designed independently from the main PA. The load impedance presented to the control PA device through its OMN is assumed to be some $R_c + jX_c$, with an arbitrary phase shift θ_c between the transistor and the hybrid coupler. Using (5) and (12) we can write the control PA drain current current I_{ds_c} as:

$$I_{ds_c} = j\frac{I_{\max}}{2}\frac{Z_{\max} - Z_{\text{bo}}}{\sqrt{2R_{\text{bo}}R_c}}e^{j(\theta_{\text{OMN}}+\theta_c)} \quad (17)$$

The maximum power $P_{c_{\max}}$ needed from the control PA to support the LMBA operation can be related to the maximum power of each main transistor as:

$$P_{c_{\max}} = P_{m_{\max}}\frac{|Z_{\max} - Z_{\text{bo}}|^2}{2R_{\max}R_{\text{bo}}} \quad (18)$$

The correct phase and turn-on point can both be controlled by an appropriate input signal and gate bias. The transistor T_c size, its drain voltage V_c and drain impedance Z_c can be chosen freely by the designer to achieve highest efficiency at the power level $P_{c_{\max}}$.

Because it drives a fixed impedance, the control PA does not contribute LMAM or LMPM distortion to the overall LMBA. Furthermore, contributions by the control PA to the overall AMAM or AMPM characteristics are straightforward to estimate based on load-pull data. In the following discussion, we ignore AMPM effects introduced by the control PA, but note that they can be compensated for using the presented techniques.

III. LOAD TRAJECTORY SELECTION

Based on the above analysis it is clear that the selected load trajectory will influence the LMBA linearity. Similarly, it is well known that load trajectory will determine the PA efficiency. Conventional load modulation assumes that a resistive load modulation is desirable [3], [40]. On the other hand, from (15)–(16) we observe that the AMPM distortion for a purely real load modulation is reduced to the intrinsic phase distortion of the branch transistor (Θ_{bo}). If an appropriate reactive component to $Z_{\max}$ and/or Z_{bo} is introduced, it can compensate for the intrinsic LMPM, leading to negligible net phase distortion at the output of the LMBA, while also affecting efficiency.

A. TRAJECTORY EFFECT ON AMPM DISTORTION

Fig. 2 presents seven different load impedance trajectories selected to explore the contributions of the load trajectory on amplitude and phase distortion and illustrate (15)–(16). Each trajectory has the same resistive component at the start

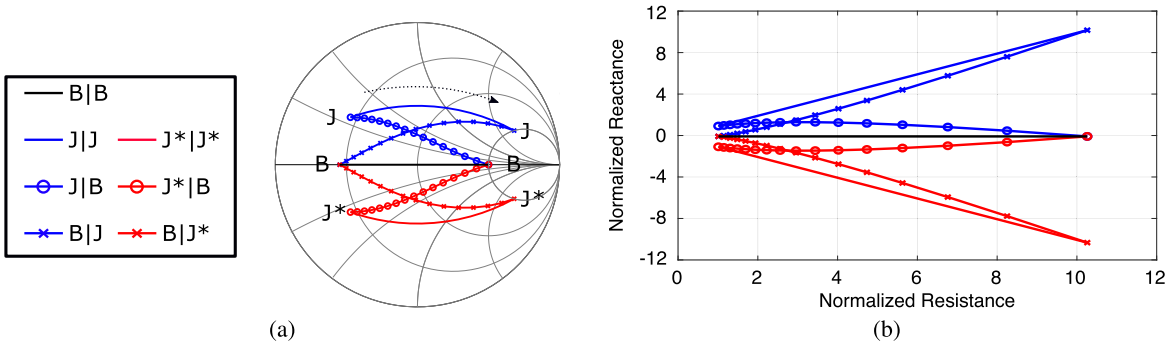

FIGURE 2. The seven load trajectories compared in this section: B | B (black), J | J and J *| J* (solid blue and red), B | J and B | J* (blue and red, cross markers), and J | B and J *| B (blue and red, circle markers), presented in the (a) Smith chart, and (b) impedance plane.

(maximum power) and end point (back-off power), but with different reactive components. We compare these modulation types which we name based on the starting and ending impedance as follows:

- **B | B**: (black curve) representing a purely resistive load modulation
- **J | J and J*|J***: (solid blue and solid red) with a fixed reactance to resistance ratio, expressed by

$$Z(\beta) = \frac{1}{\beta}(1 + j\delta) \tag{19}$$

- **B | J and B | J***: (blue and red, cross markers) in which the reactance to resistance ratio varies from 0 to δ, according to

$$Z(\beta) = \frac{1}{\beta} + j\delta\frac{\beta_o - \beta}{\beta_o - 1} \tag{20}$$

- **J | B and J*|B**: (blue and red, circle markers) in which the reactance to resistance ratio varies from δ to 0, according to

$$Z(\beta) = \frac{1}{\beta} + j\delta\frac{\beta - 1}{\beta_o - 1} \tag{21}$$

In these equations, the parameter δ represents the relative value of the reactance, and takes the value of either 1 (J family of trajectories) or -1 (J* family of trajectories). β_{bo} is chosen in each case to produce 12 dB of dynamic range, according to (14). The drive parameter β is swept over β_{bo} to 1, producing the load modulation trajectories. We note that the naming convention used here is based on that of the B-J mode continuum [34].

The analysis in this section is based purely on the fundamental-frequency load trajectory, and assumes that the second harmonic termination has only a small effect on the AMPM response. This assumption is validated in the simulations presented in Section IV. In other words, the fundamental-frequency trajectory may first be selected for linearity, and then the appropriate harmonic termination is chosen to maximize efficiency. Furthermore, we note that while the continuous modes of operation are typically associated with wide bandwidth PAs [27], [34], in this work we focus solely on linearity and efficiency at the design frequency. Previous work [16] has demonstrated that harmonic termination influences performance in load-modulated architectures even when bandwidth is not considered.

Fig. 3(a) and (b) plot the AMAM and AMPM of the LMBA versus the back-off range for each trajectory. They are computed according to (14)–(16) assuming $G_{m1_{\max}}/G_{m1_{\text{bo}}} = 1$ and $\Theta_{\text{bo}} = 0$. In other words, only the contribution of the load trajectory is plotted. We see that the AMAM is similar for all trajectories and increases as we get into higher back-off ranges. Referring to (14)–(16), the AMAM can be written as:

$$\text{AMAM} = \gamma\beta_{\text{bo}} \tag{22}$$

Since each of the seven trajectories have identical resistive components at the starting and ending points, and therefore the same β_{bo}, the gain compression is independent of the load trajectory. The AMPM, on the other hand, ranges from 0° (B | B trajectory) to ±40° (B | J or B | J* trajectories) at 12 dB back-off. It is interesting to note that while the J | B and J*|B trajectories appear somewhat opposite to the B | J and B | J* in the Smith chart, their resulting AMPM effects are comparatively small. This can be understood by further expanding the AMPM expression from (16):

$$\text{AMPM} = \tan^{-1}\left(\frac{X_{\max} - X_{\text{bo}}}{R_{\max} + R_{\text{bo}}}\right) \tag{23}$$

We see that for an identical resistive component variation, the AMPM of the LMBA is defined by the absolute difference in reactance. Therefore, the preferred strategy to compensate for the intrinsic LMPM distortion of the branch amplifier is to introduce reactive loading at the back-off impedance.

B. TRAJECTORY SELECTION FOR EFFICIENCY

The design considerations presented above do not take into account the performance of the amplifier for the different impedance trajectories, and are independent of other parameters such as second harmonic termination. Yet we know that the load presented to the transistor will determine the overall performance, both in the distortion terms $G_{m1_{\max}}/G_{m1_{\text{bo}}}$ and Θ_{bo}, and in terms of the PA efficiency and output power. In order to exploit the conclusions of the previous section, a load

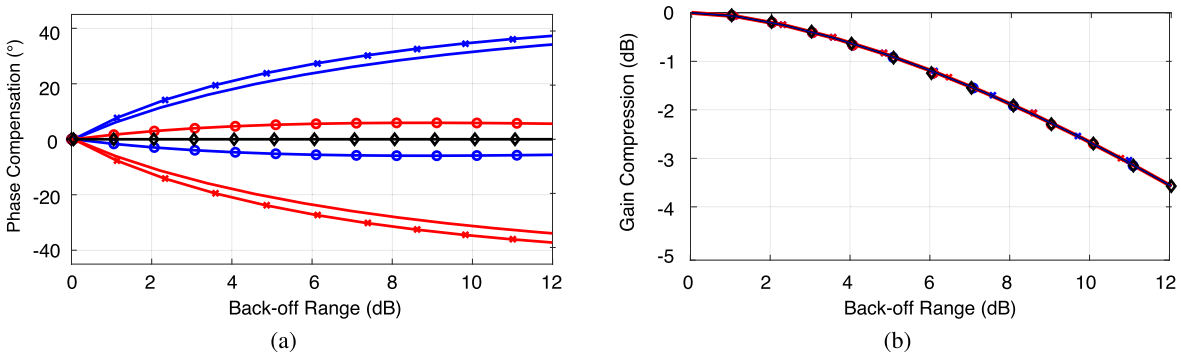

FIGURE 3. (a) Phase compensation due to load modulation and (b) gain compression versus γ for the different load trajectories presented in Fig. 2, calculated from (14)–(16).

trajectory solution is needed in which AMPM distortion is zeroed while high efficiency is maintained.

The starting and ending points of the trajectories in Fig. 2 correspond to impedances falling within a continuous operating mode [34]. Therefore, by allowing the second harmonic termination to include reactive termination according to continuous mode theory, the design space is expanded. The design factor δ ($|\delta| \leq 1$) relates the now complex terminations at the fundamental and second harmonic as:

$$Z_{opt,f0} = R_{opt}(1 + j\delta) \tag{24}$$

$$Z_{opt,H2} = -j\frac{3\pi}{8}\delta R_{opt} \tag{25}$$

$$R_{opt} = \frac{(V_{DS} - V_K)^2}{2P_{m1,2_{\text{bo}}}} \tag{26}$$

A value of $\delta = 0$ corresponds to class B, while $\delta = 1$ and $\delta = -1$ are termed class J and J* respectively. According to the theory, the efficiency and output power of an amplifier is identical for any value of δ. Therefore the PA efficiency can be maximized at any one of the starting or ending points of the load trajectories in Fig. 2 by appropriately terminating the second harmonic. We note that in this work, because load modulation is applied at the fundamental only, ideal continuous mode operation is not maintained over the fundamental load modulation [16].

IV. LMBA DESIGN METHODOLOGY

Based on the observations in Sections II and III, we present a generalized LMBA design methodology focusing on AMPM mitigation through load trajectory selection. Whereas the effects of load trajectory can be described analytically, both the efficiency and the intrinsic LMAM and LMPM of the transistor are best evaluated by simulated or measured load-pull. Furthermore, if some control PA efficiency can be assumed, load-pull data from a single-ended transistor used in the main PA is sufficient to estimate the overall AMAM, AMPM and efficiency of the entire LMBA architecture.

In the proposed design procedure, once the optimum peak-power and back-off power impedances are selected, the power required from the control amplifier is calculated and the constituents of the LMBA can be designed. This approach differs from that in [6] in that the harmonic termination is not assumed to be fixed, enabling control of AMPM distortion with limited effect on efficiency. The methodology is summarized as follows:

1) **Main transistor selection**. This choice is based on the required maximum power $P_{m_{\max}}$. We see from (13) that this power depends on the load trajectory, which is still to be determined. As an initial approximation we can consider the case where both Z_M and Z_{bo} are purely real. $P_{m_{\max}}$ then depends only on the overall output power and back-off range:

$$P_{m_{\max}} = P_{L_{\max}}\frac{2\sqrt{\gamma} - 1}{2\gamma} \tag{27}$$

2) **Load-pull and trajectory selection:**
   - **The second harmonic termination** is first selected, with multiple different harmonic terminations compared. The fundamental and second harmonic impedances at the intrinsic drain plane can be calculated according to (24)–(25) for a particular value of δ. In cases without access to the intrinsic drain plane, a more thorough study has to be done in which the second harmonic termination is swept with, for example, $|\Gamma| = 0.95$.
   - **Stability and input match:** A parallel RC network is designed to stabilize the transistor loaded with the previously found impedances. The input impedance is then matched to 50 Ω with an additional input matching network (IMN). In this work, different IMNs are designed for the three example PAs.
   - **The fundamental impedance** presented to the transistor's drain is finally swept. In this work, reflection coefficient magnitudes up to 0.8 relative to the previously found fundamental-frequency termination are simulated. An input power sweep is performed for each impedance and the predicted back-off range, maximum power, AMAM/AMPM distortions and drain efficiency of the LMBA are calculated from

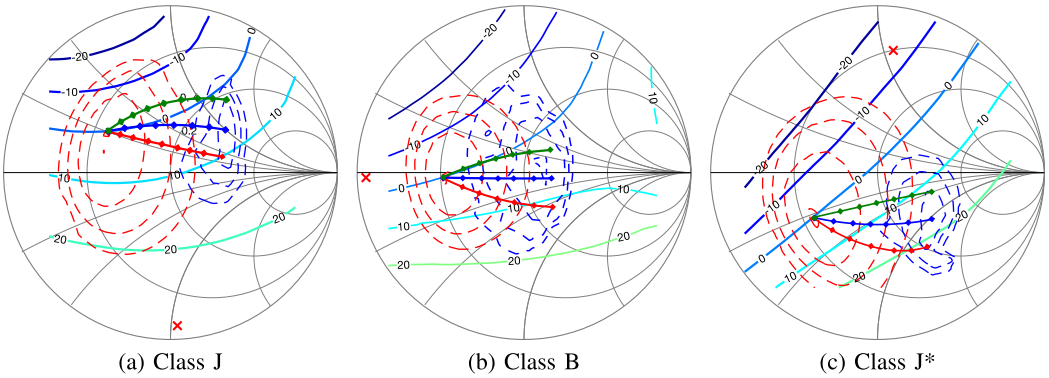

(a) Class J (b) Class B (c) Class J*

FIGURE 4. Results of the load-pull measurements for class J/B/J* modes. The solid contours represent contours of constant intrinsic phase distortion. The dotted red and blue contours show respectively the maximum power and maximum efficiency at back-off. The red cross marks the second harmonic termination. The diamond markers represent the selected load trajectories, i.e. the nominal J | J, B | B, and J *| J* trajectories (blue), increased reactance to resistance ratio at back-off (green), and decreased ratio (red).

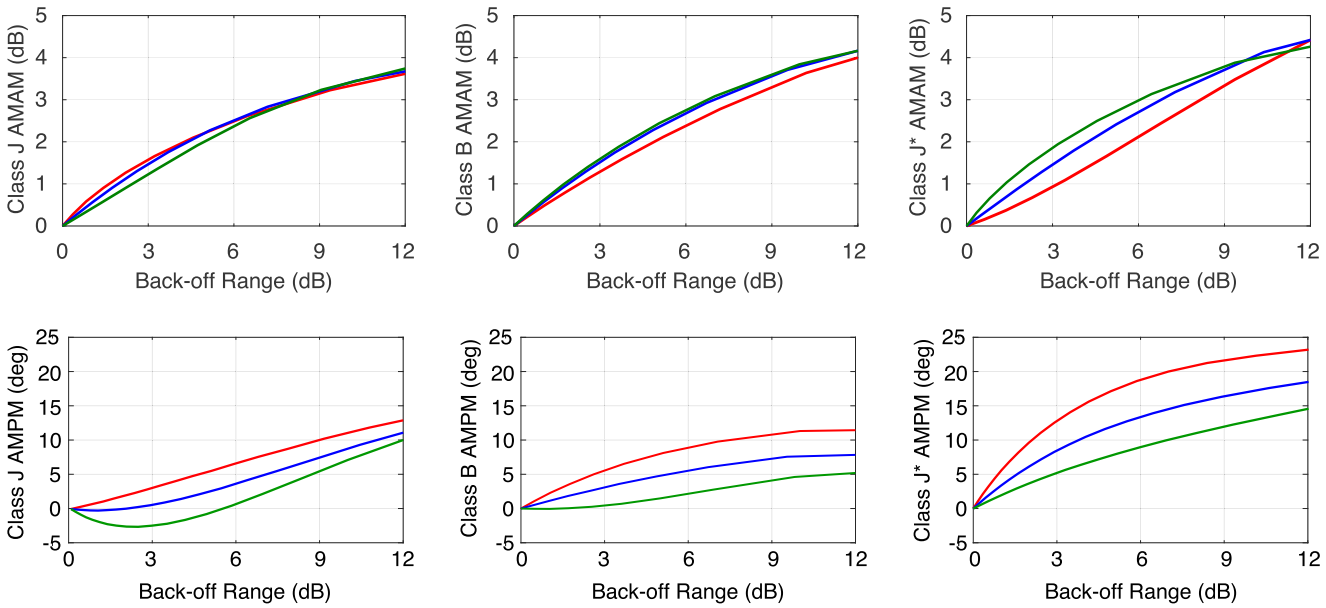

FIGURE 5. Estimated overall phase and amplitude distortion of an LMBA based on (15)–(16) and the load-pull data. In order to capture the distortion due to the load modulation only, the transistor is operated with a low input power of 15 dBm.

(14)–(16). If the results are not satisfactory the second harmonic can be re-tuned and the load-pull repeated.

3) **Control transistor selection.** With the back-off and maximum impedance chosen, $P_{c_{\max}}$ can be found from (18). We can select a device that will give the highest efficiency for the desired output power, noting that standard PA design techniques can be used for the control PA due to its fixed load impedance.
4) **Passive network design** including the OMNs and the hybrid couplers.

A. LOAD-PULL ANALYSIS EXAMPLE

Load-pull simulations of the CGH40010F GaN transistor from Cree operating at 2.4 GHz are used to illustrate the process of determining the load trajectory to minimize phase distortion while maintaining high efficiency. The transistor large-signal model provides access to the intrinsic drain plane of the device, allowing the load-pull simulations to be de-embeded as described in Section II. We compare three different scenarios for second harmonic termination: capacitive, short and inductive, i.e. according to (25) with δ equal to 1, 0 and -1. We name these three designs according to their peak-power impedance terminations, i.e. as class J, class B, and class J*. In this section we will evaluate the three different harmonic termination scenarios for various different back-off impedance termination conditions.

Figs. 4, 5, and 6 summarize the resulting load-pull data for the three modes. In Fig. 4, power contours are displayed at a fixed 2 dB compression, the center being the impedance at maximum power. The drain efficiency contours correspond to an output power fixed at $P_{m_{\text{bo}}}$ (equal to $P_{L_{\max}} - \gamma$ -3 dB).

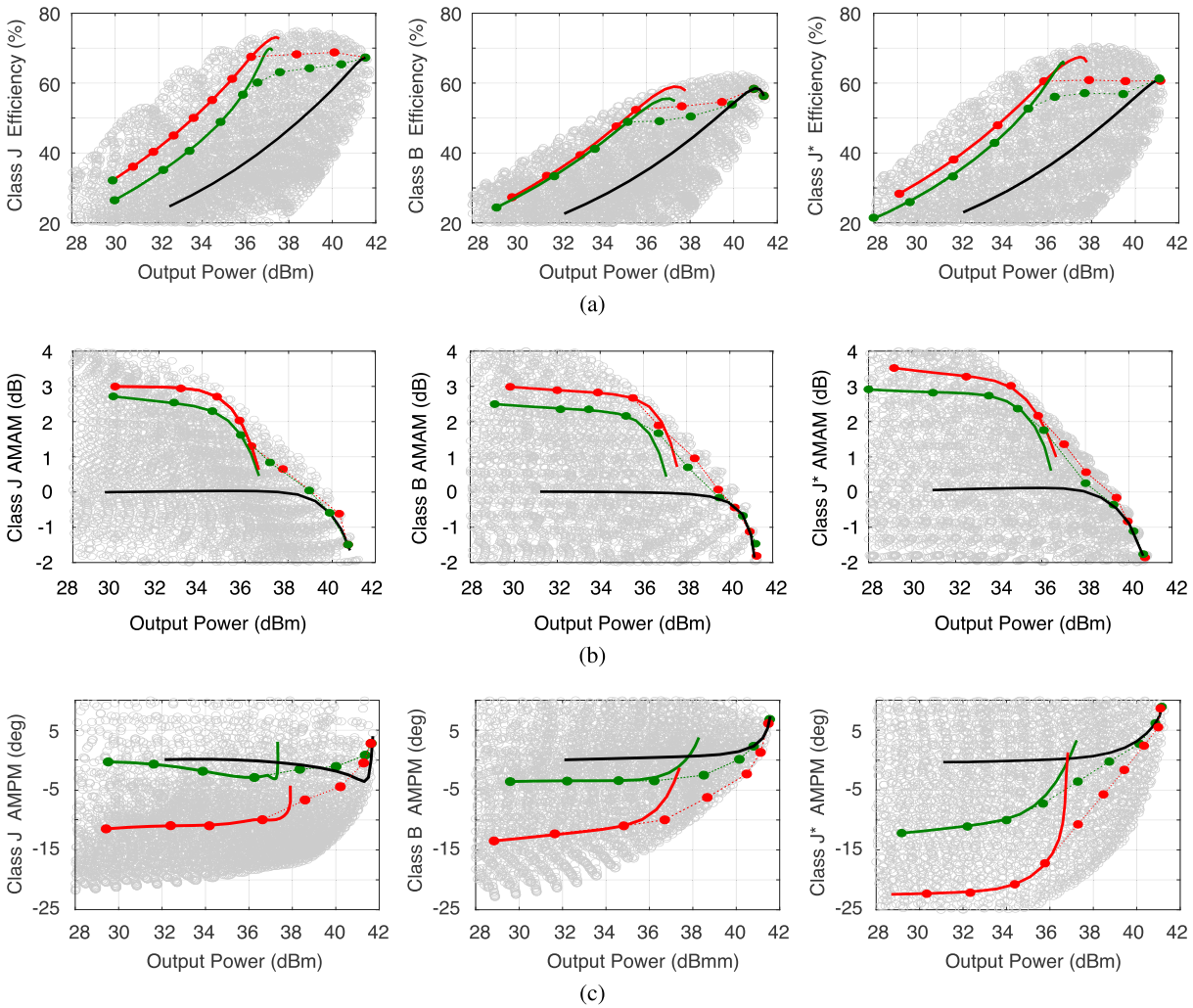

FIGURE 6. **Simulated drain efficiency, gain compression and phase distortion for the class J/B/J* operation, from left to right. The gain compression and phase distortion account for both the load-pull data and the load trajectory, according to (15)–(16). The behavior over swept input power is shown for the peak-power impedance (black curve) and for back-off impedances with increased (green) and decreased (red) reactive components for each PA class, referring to Fig. 4.**

The AMPM contours, shown in colored contours, and represent a combination of simulated and calculated behavior. To generate them, the phase of the intrinsic drain current is first simulated at each load-pull impedance at low power ($P_{\text{in}} =$ 15 dBm). The zero phase reference point is selected to be the peak-power impedance, i.e the intrinsic drain current phase for all other points is normalized to the value at the peak power impedance. The AMPM distortion of the LMBA is then calculated using (16), replacing Z_{Max} by the peak-power impedance and Z_{BO} and θ_{BO} by each load pull impedance and the corresponding normalized phase of the intrinsic drain current. With this approach, the AMPM of the complete LMBA using the specified transistor and harmonic loading is predicted from the load pull data.

The effects of the second harmonic terminations can be clearly seen, introducing the expected complex components on the optimal fundamental impedances from continuous mode theory. The AMPM distortion also changes with the operating mode but with a weaker dependence. Comparing the efficiency and AMPM contours in Fig. 4, it is apparent that a range of back-off impedances can be selected with similar efficiency performance but with an approximately 10 degree range in AMPM distortion. To illustrate this effect we consider three load trajectories introducing different reactive to resistive ratios for each of the three PA classes.

In the blue trajectories the reactive to resistive ratios at peak power and back-off are equal, while in green/red this ratio becomes bigger/smaller in back-off. From Fig. 4 it can be seen that the back-off efficiencies of all three trajectories will be similar. Fig. 5 presents the predicted AMPM and AMAM of the LMBA versus the back-off power for each of these load trajectories. As in Fig. 4, these figures account for both the load-pull data and the load trajectory according to (15)–(16). The results in Fig. 5 show that the AMPM distortion depends

strongly on the selected load trajectory. For the B and J cases, we can find optimum impedances that minimize the phase variation, reaching only 6 degrees of distortion at 12 dB back-off. The class J* case on the other hand shows greater than 15 degrees of AMPM for all cases. In contrast, the AMAM does not seem to depend as much on the load trajectory, with a worst-case variation of 1 dB in the J* case.

When input power variation is included in the simulation, the resulting performance is as seen in Fig. 6. Here, simulations are performed for the three different harmonic terminations at each load-pull impedance point with input power ranging from 15 to 35 dBm to generate each grey point in the "cloud". The highlighted curves show the device performance over input power for three different drain impedances: the drain impedance that produces maximum output power according to Fig. 4 (black curve), and for the two back-off impedances corresponding to the decreased and increased reactance to resistance ratio impedances in Fig. 4 (red and green curves). Dashed lines represent the extrapolated performance of the load modulated amplifier, plotted by tracking the 1 dB compression point of each curve found over the load trajectory. Fig. 6(b) and (c) are plotted based on (15)–(16), where Z_{Max} and $G_{m1_{\max}}$ are the previously described peak-power impedance and corresponding gain, Z_{bo} each load-pull impedance and $G_{m1_{\text{bo}}}$ and θ_{bo} the corresponding gain and phase of the intrinsic drain current. While all three cases reach similar maximum power levels, their drain efficiencies are not equal: the class J design reaches up to 75% drain efficiency, while the class B and class J* reach only 63% and 70%, respectively. This is in accordance with [41], where the $\delta = 1$ solution (class J) produced greater efficiencies at back-off.

Two conclusions can be drawn from the load-pull data. Referring to the class J results in Fig. 6, we see that by sacrificing 8 percentage points of drain efficiency, the AMPM distortion can be drastically reduced, from 12 degrees to 3 degrees. The AMAM performance is largely unaffected by the selection of PA operating class. These results confirm what was observed in Fig. 5. The second conclusion is that when taking into account both the drain efficiency and the phase distortion, the class J PA appears superior to the other cases.

B. INPUT SIGNAL GENERATION

The remaining aspect of the LMBA design to be considered is the input signal generation: dual-input [20] or RF-input [21]. In a dual-input system, both the main and the control PA are biased at or slightly above the device threshold voltage. The correct relative amplitude and phase is generated digitally, including any corrections required to compensate for AMAM and AMPM non-linearities in the control PA. In this case the main and the control PAs are designed separately and connected through the output hybrid coupler. The dual-input LMBA carries the same advantages of a dual-input Doherty [42]–[44], while also allowing for the load modulation trajectory to be adapted after fabrication.

In the RF-input case, the control amplifier is biased in class C. An input splitter is added to feed the main and control amplifiers. This system offers reduced operating complexity, but requires the design of a fixed input splitter with a given splitting ratio and phase delay. In a general case, the inputs of each main transistor and of the control transistor can be modeled as:

$$\begin{aligned} P_{in_{m1,2}} &= d_{pm}\frac{P_{in}}{2} \\ P_{in_c} &= (1-d_{pm})P_{in} \end{aligned} \tag{28}$$

where d_{pm} is the split ratio. The maximum power of the control amplifier can be rewritten in terms of the input power and the gain of each device, which can be found from the load-pull data for a given impedance:

$$P_{in_c}G_c = G_m P_{in_{m1,2}}\frac{|Z_{\max}-Z_{\text{bo}}|^2}{2R_{\max}R_{\text{bo}}} \tag{29}$$

Combining equations (28) and (29) the power division ratio can be written as:

$$d_{pm} = 2\frac{G_c}{G_m}\frac{1}{\frac{|Z_{\max}-Z_{\text{bo}}|^2}{2R_{\max}R_{\text{bo}}}+2\frac{G_c}{G_m}} \tag{30}$$

As described in [21], a phase offset may also be required to compensate for different phases in the main and control paths. This can be implemented by inserting a network with the required phase response in either the main or control path depending on the sign of the required phase offset.

V. LMBA PROTOTYPE DESIGN

Following the process above, we design example linear LMBAs operating at 2.4 GHz with a maximum output power of 46 dBm and a 6-dB back-off range. In order to validate the presented theory three amplifiers are designed, with harmonic terminations corresponding to J, B and J* classes. The CGH40010F device is used and the design is based on the simulated load-pull performance presented in the previous section. From (13) we estimate the main transistors' maximum and back-off powers to be $P_{m1,2_{\max}} = 41.75$ dBm, $P_{m1,2_{\text{bo}}} = 37$ dBm, indicating that this device will meet the output power requirements.

A. MAIN PA DESIGN

For each of the three PA classes, the impedance $Z_{\max}$ is chosen to produce the maximum power (i.e. center of the maximum power contours) and Z_{bo} is selected from Fig. 6 to give the best linearity/efficiency compromise. The resulting parameters are calculated from (13)–(14) and (18) and summarized in Table 1. The OMNs set the second harmonic impedance using a shunt open stub. The rest of the OMN is a T-network to match the fundamental back-off impedance to 50 Ω. The drain supply voltage is provided through a quarter wavelength line positioned after the second harmonic stub in order not to affect the fundamental or second harmonic impedances.

TABLE 1. Powers and Impedances Selected for the Three Different Classes of Operation for the Main PA. For Each Case, $P_{m_{bo}} = 37$ dBm

	$P_{m_{max}}$	$P_{c_{max}}$	$P_{L_{bo}}$	$P_{L_{max}}$	γ	Z_{bo}	Z_{max}
J	41.5	40.2	40	45.9	5.9	59 + j23	20 + j9
B	41.6	39.6	39.8	45.8	5.8	50 + j4	17 - j
J*	41.3	40.7	39.9	45.9	5.9	53 - j20	16 - j10

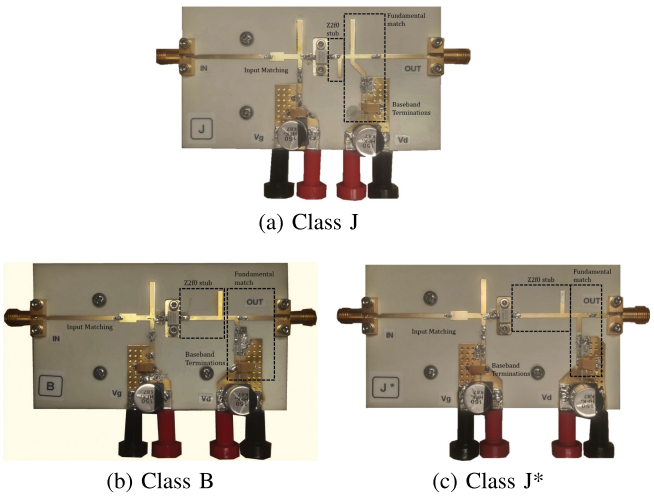

(a) Class J

(b) Class B (c) Class J*

FIGURE 7. Photographs of the three main PA designs.

All PAs are stabilized with the same parallel RC network, and the input conjugately matched to the appropriate impedance depending on the output harmonic termination. Fig. 7 shows photographs of the three PA designs, fabricated on 0.762 mm Rogers 4350B substrate.

B. LMBA OPERATION

So far the design procedure has been based on finding the optimal maximum impedance and then choosing the back-off impedance based on the linearity/efficiency trade-off. Now that the PAs are manufactured, the back-off impedance is fixed by the OMN. We have to perform the opposite operation of finding an optimum maximum-power impedance for the design. This is done by selecting the fixed phase offset between the main and control PAs.

In the LMBA operation, we use the same PA design (i.e., the same operating class) for the balanced and control PAs in each case. The drain voltages were adapted to meet the power requirements of Table 1, with the main PAs biased at 24 V and the control PA at 28 V. Fig. 8 presents the simulated pseudo-RF-input performance of each LMBA, when ideal hybrid couplers are assumed. The reported gain and efficiency of the LMBA account for the contributions of both the main and control amplifiers:

$$\text{Gain} = 10\log\left(\frac{P_L}{P_{in_{m1,2}} + P_{in_c}}\right) \tag{31}$$

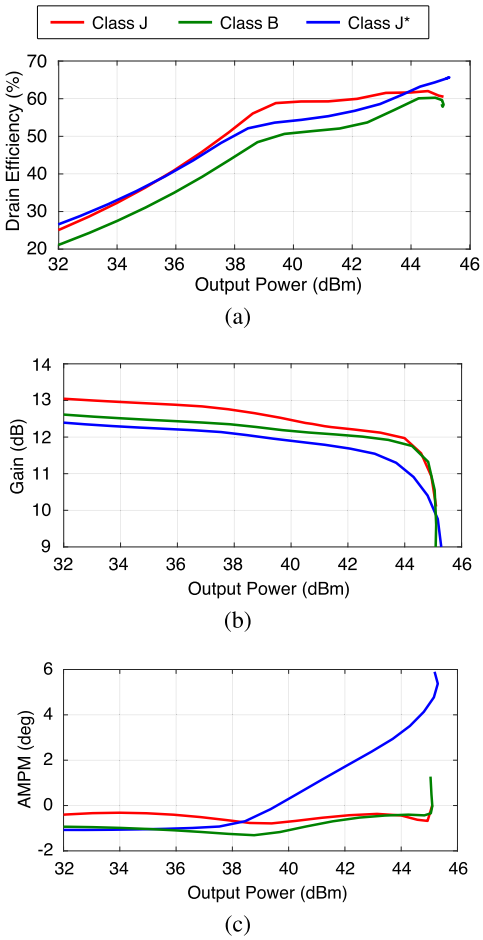

FIGURE 8. Simulated performance for each LMBA, showing the performance of the entire LMBA, i.e. including both the main and control PAs. (a) – Drain efficiency, (b) – gain and (c) – phase distortion versus output power.

$$\text{DE} = 100\frac{P_L}{P_{DC_{m1,2}} + P_{DC_c}} \tag{32}$$

where P_L represents the output power of the LMBA, $P_{in_{m1,2}}$ and P_{in_c} the input power of the main and control amplifiers and $P_{DC_{m1,2}}$ and P_{DC_c} the dc power consumed by the main and control amplifiers.

The simulations match well to the results predicted from Fig. 6. The class-J LMBA presents the best compromise of linearity and efficiency, with 60% drain efficiency at 6 dB back-off and less than 2 degrees of AMPM distortion. We also observe the very high phase distortion of the class-J* LMBA and the lower drain efficiency of the class-B LMBA. We notice that the maximum output power is 0.8 dB lower than predicted. This can be explained from Fig. 9, which shows the load trajectory and the second harmonic termination for each case. All three trajectories change direction when the transistors approach compression, resulting in lower maximum power. This effect is due to the AMPM distortion of all three transistors (including the control PA), which changes the

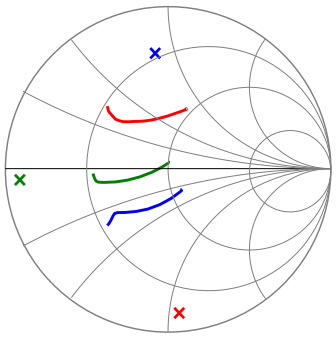

FIGURE 9. Simulated load trajectories for each LMBA. Crosses represent the corresponding second harmonic termination.

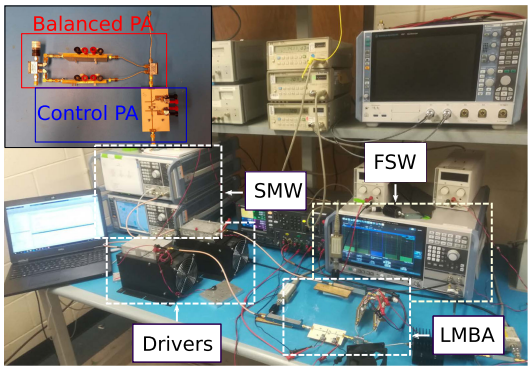

FIGURE 10. Photograph of the experimental test setup, with inset showing detail of LMBA under test.

relative phase relationships as the PAs compress. It was also observed in [22].

VI. MEASUREMENT

The experimental setup is shown in Fig. 10. Connectorized hybrid couplers from Minicircuits (ZX10Q-2-27-S+) are used, which is measured to have an insertion loss of 0.75 dB, large compared to a typical microstrip design. The design is operated as a pseudo-RF-input system, i.e. with a fixed phase offset. This configuration gives extra degrees of freedom, as the relative power and phase of the two ports can be adapted to produce different load trajectories. For CW testing, two synchronized Rhode & Schwarz SMW200A signal generators are used to generate the main and control input signals. A Rohde & Schwarz FSW40 Signal Analyzer is used to record the output.

The testing procedure has two steps. In an initial characterization, the control amplifier is turned off, and the performance of the balanced amplifier without load modulation is recorded. In the second step, the relative phase and amplitude of the control PA's input is swept for each main PA input power level. This produces effectively a load-pull of the balanced amplifier and we can determine the optimal impedance presented for peak output power. During this test the control amplifier is the same as the one used as the main device and is biased at the threshold voltage. The result of these measurements is

TABLE 2. Measured Results for Each Amplifier and Load Trajectory With Modulated Signals

Phase Offset (°)	Class J		Class B		Class J*	
	Linear	Eff.	Linear	Eff.	Linear	Eff.
	170	190	120	140	90	110
DE (%)	40.5	44	33	36	38	40
Gain (dB)	10.6	10.3	9.8	9.6	10	9.9
ACLR (dBc)	-40.5	-33	-38.5	-31	-33	-31

the cloud of points seen in Fig. 11. Two trajectories are selected, corresponding to different fixed phase offsets between in the main and control PA input signals: one for maximum efficiency (in red) and the second representing a linearity-efficiency compromise (green). For each class of PA, the two trajectories have 20° of phase difference.

The black dotted lines in Fig. 11 show the simulated performance, reproduced from Fig. 8. It can be seen that all three designs have 1–2 dB lower gain than expected from simulation; this is a difference that we have previously experienced with this family of devices [16], [21], [22]. Likewise, 1–2 dBm lower output power is observed. The AMPM response overall matches with the predicted trends from simulation, with the class J LMBA matching very closely and the class B and J* exhibiting similar characteristics but at different power levels than expected. Specifically of interest is the behavior of the LMBA in the load-modulated region, because the LMBA architecture does not affect the main PA performance in back-off where the control PA is off and the main PAs operate into a fixed load. As expected, the class J PA presents the best compromise, achieving higher efficiency than the other cases with a particularly flat AMPM. Note that all measurements — efficiency, gain and output phase — include the effects and power consumption of both the balanced and control PAs.

Modulated measurements are next performed and the two relative phase settings for efficiency and linear-efficient compromise are compared for each class of operation. An 8.6 dB PAPR LTE signal with 10-MHz bandwidth is used. The control PA again uses the same design as the main PA, but is biased below pinch-off (i.e., in class C). The gate bias of the main amplifier is adjusted in order to minimize the ACPR. The two signal generators' baseband generators are synchronized and time-aligned with an external oscilloscope and the two input signals have the same amplitude. Table 2 summarizes the measurement results for all cases. We note that the 0.75-dB insertion loss of the output coupler degrades the overall LMBA performance. Assuming an approximately 0.5-dB improvement with a microstrip design, we estimate the back-off and maximum efficiency would improve by 5 percentage points.

The best-performing LMBA is identified as the class-J version operating with a fixed relative phase offset of 170 degrees (so-called linear mode). This configuration achieves −40.5 dBc ACLR with 40.5% drain efficiency at 35.2 dBm average output power. Fig. 12 shows dynamic AMAM and AMPM measurements for this LMBA when excited by the

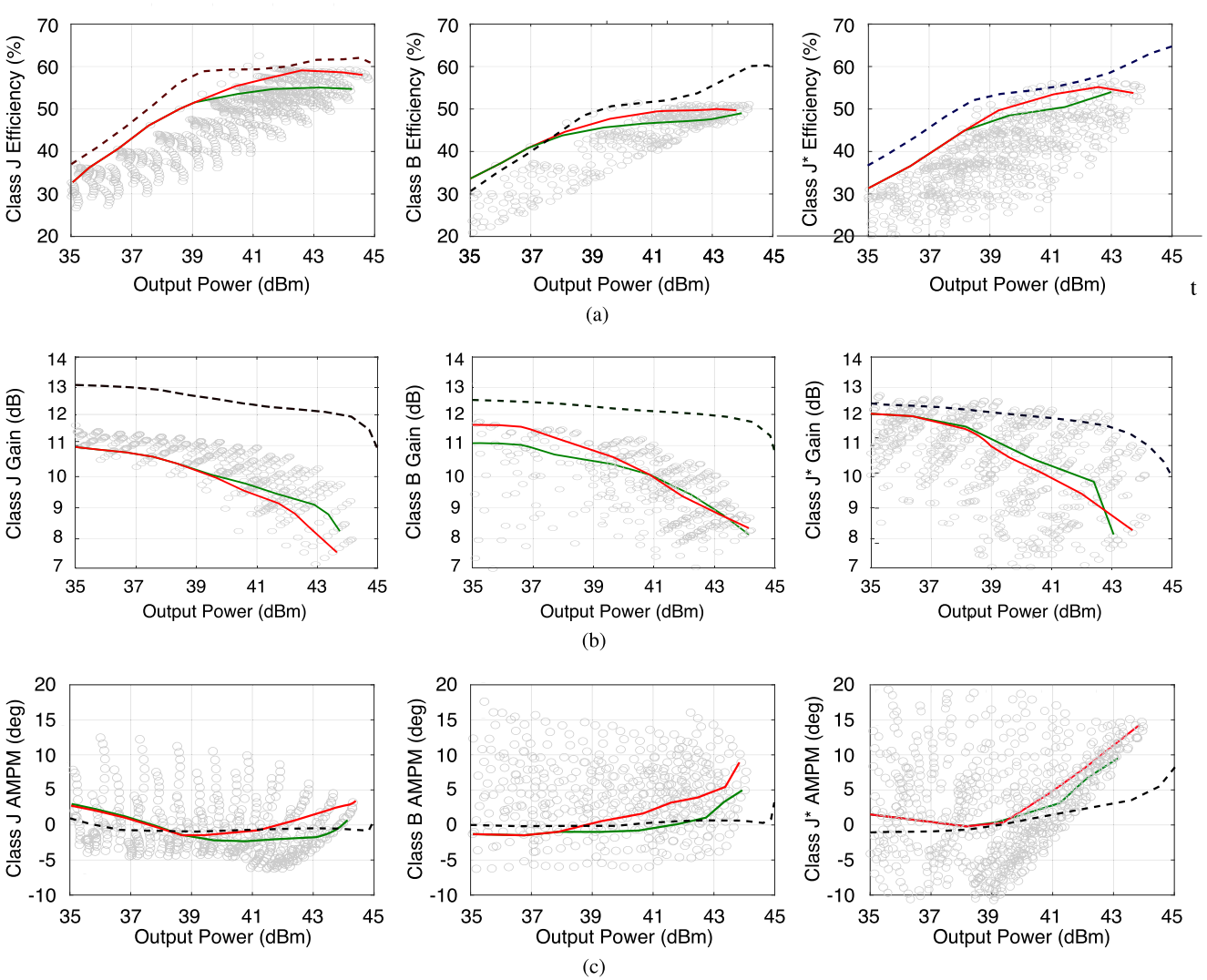

FIGURE 11. **Measured CW performance of the class J, B and J* LMBA, showing the performance of the entire LMBA, i.e. including both the main and control PAs. From left to right: drain efficiency, gain and phase distortion versus output power. The simulated result, assuming an ideal lossless hybrid combiner, is shown for comparison (black dashed line).**

LTE signal without linearization, compared to the measured CW results. The different characteristic is attributed to the CW measurement method, in which input power is swept from low to high, resulting in greater self-heating at the higher output power levels compared to in the modulated tests.

Finally, the class-J LMBA amplifier was linearized using a memory polynomial of 4th order and a memory depth of 2 samples. The resulting system achieved at 35 dBm average output power −48 dBc ACLR with 39.8% drain efficiency, or 44.8% when the coupler's losses are de-embedded. Fig. 13 shows the unlinearized spectrums measured with the class-J LMBA for a phase of 170° and 190° degrees, and in blue the linearized spectrum for a phase offset of 170°. Although the ACLR of this LMBA may not be sufficient in all applications to operate without output power back-off or DPD, it is notable that the class J LMBA performs with not only 2 dB better ACLR than the class B case, but with 7 percentage points higher efficiency, and without sacrificing output power. In other words, the LMBA performance can clearly be improved simply by the harmonic impedance selection and complex load trajectory proposed here.

Table 3 shows a comparison summary of the LMBAs presented in this work and state-of-the-art GaN PAs with similar operating frequency and power level. Compared to the other presented RF-input LMBA works, the class-J pseudo RF-input LMBA presented here demonstrates 13–15 dB better ACLR before DPD, operating with similar performance to a dual-input LMBA with reduced signal complexity. The reported drain efficiencies are competitive with the state of the art, particularly when the additional loss of the connectorized coupler, which degrades efficiency by approximately 5 percentage points, is considered.

TABLE 3. Comparison to State-of-the-Art GaN Load-Modulated Power Amplifiers

Ref.	Architecture	Center Freq. (GHz)	Inst. BW (MHz)	PAPR (dB)	Avg Pwr (dBm)	Eff. (%)	ACLR (dBc)
[6]	DPA	2.14	10	8.6	35.5	44	-40.8 / -47.9†
[9]	DPA MMIC	2.3	10	7.2	35.3-33.7	45.5	-35.6
[10]	DPA-Linearizer	0.8	20	7.1	33	33.2*	-42.5
[11]	DPA	3.5	10	8.4	34.5	42.4	-37
[12]	DPA	5	40	7.4	32	42	-43.8 / -51.3†
[20]	Dual-input LMBA	1.7–2.5	5	9	39.4-40	43-46*	-39 / -53†
[25]	Sequential LMBA	3.05–3.55	40	8	35.5	57.8	-46.7†
[21]	RF-input LMBA	1.8–3.8	3.84	9	31–32	17–26*	-26 / -30
[22]	RF-input LMBA	2.4	10	7.5	38	47	-27
[27]	RF-input CM-LMBA	1.45–2.45	100	8	37.8	45.6*	-31.5 / -47†
This Work	Class J* LMBA	2.4	10	8.6	35.5	38	-33
	Class B LMBA				35.5	33	-38.5
	Class J Efficient				35.5	44	-40.5
	Class J Linear				35.5	40.5 / 39.8†	-40.5 / -48†

†Including DPD, *PAE

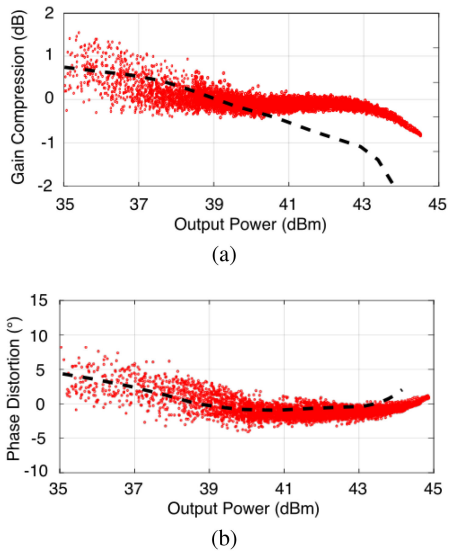

FIGURE 12. Dynamic AMAM and AMPM measurements of the class J LMBAs for a 10 MHz, 8.6 dB PAPR LTE signal. The CW measurement is shown for comparison (dashed black line).

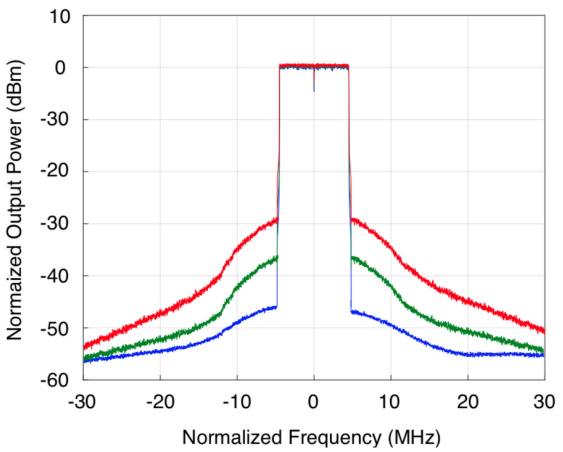

FIGURE 13. Class J LMBA spectrum, for a fixed phase offset of 190° (red) and 170° (green). In blue is the spectrum with 170° offset after applying DPD.

VII. CONCLUSION

In this paper the impact of the load trajectory on the AMPM distortion of an LMBA is studied. It is shown that by appropriately terminating the second harmonic, very high efficiency can be obtained while keeping a nearly flat AMPM. This approach broadens the LMBA design space and allows new solutions with an improved efficiency/linearity trade-off.

A data driven design methodology is presented whereby the performance of the entire LMBA system can be accurately predicted by load-pulling a single ended device. This is possible because the control amplifier is isolated and drives a fixed load. The methodology is experimentally demonstrated by designing from load-pull data three LMBAs with different second harmonic terminations. The best linearity/efficiency compromise is found with the class-J LMBA, where 40.5% drain efficiency and −39.6 dBc ACLR are achieved with a 10 MHz 8.6 dB PAPR signal at 2.4 GHz.

REFERENCES

[1] A. N. Lozhkin, T. Maniwa, and H. Ishikawa, "New low power digital sub-band predistorter for OFDM signals," in *Proc. Int. Symp. Wireless Pers. Multimedia Commun.*, 2019, pp. 1–6.

[2] C. Fager, T. Eriksson, F. Barradas, K. Hausmair, T. Cunha, and J. C. Pedro, "Linearity and efficiency in 5G transmitters: New techniques for analyzing efficiency, linearity, and linearization in a 5G active antenna transmitter context," *IEEE Microw. Mag.*, vol. 20, no. 5, pp. 35–49, May 2019.

[3] S. C. Cripps, *Advanced Techniques in RF Power Amplifier Design*. Norwood, MA, USA: Artech House, 2002.

[4] Y. Cho, D. Kang, J. Kim, K. Moon, B. Park, and B. Kim, "Linear Doherty power amplifier with an enhanced back-off efficiency mode for handset applications," *IEEE Trans. Microw. Theory Techn.*, vol. 62, no. 3, pp. 567–578, Mar. 2014.

[5] S. M. M. Jafari and H. Shamsi, "Linear Doherty power amplifier with enhanced back-off efficiency mode for LTE applications," in *Proc. Iranian Conf. Elect. Eng.*, 2016, pp. 1724–1728.

[6] W. Hallberg, M. Özen, D. Gustafsson, K. Buisman, and C. Fager, "A Doherty power amplifier design method for improved efficiency and linearity," *IEEE Trans. Microw. Theory Techn.*, vol. 64, no. 12, pp. 4491–4504, Dec. 2016.

[7] R. Giofré, L. Piazzon, P. Colantonio, and F. Giannini, "A distributed matching/combining network suitable for Doherty power amplifiers covering more than an octave frequency band," in *Proc. IEEE Int. Microw. Symp.*, 2014, pp. 1–3.

[8] R. Giofrè, L. Piazzon, P. Colantonio, and F. Giannini, "A closed-form design technique for ultra-wideband Doherty power amplifiers," *IEEE Trans. Microw. Theory Techn.*, vol. 62, no. 12, pp. 3414–3424, Dec. 2014.
[9] S. Jee, Y. Park, Y. Cho, J. Lee, S. Kim, and B. Kim, "A highly linear dual-band Doherty power amplifier for femto-cell base stations," in *Proc. IEEE Int. Microw. Symp.*, 2015, pp. 1–4.
[10] Y. Hu and S. Boumaiza, "Doherty power amplifier distortion correction using an RF linearization amplifier," *IEEE Trans. Microw. Theory Techn.*, vol. 66, no. 5, pp. 2246–2257, May 2018.
[11] H. Lyu and K. Chen, "Balanced-to-Doherty mode-reconfigurable power amplifier with high efficiency and linearity against load mismatch," *IEEE Trans. Microw. Theory Techn.*, vol. 68, no. 5, pp. 1717–1728, May 2020.
[12] X. Fang, A. Chung, and S. Boumaiza, "Linearity-enhanced Doherty power amplifier using output combining network with predefined AM-PM characteristics," *IEEE Trans. Microw. Theory Techn.*, vol. 67, no. 1, pp. 195–204, Jan. 2019.
[13] H. Chireix, "High power outphasing modulation," *Proc. Inst. Radio Eng.*, vol. 23, no. 11, pp. 1370–1392, 1935.
[14] M. Özen, M. van der Heijden, M. Acar, R. Jos, and C. Fager, "A generalized combiner synthesis technique for class-E outphasing transmitters," *IEEE Trans. Circuits Syst. I, Reg. Papers*, vol. 64, no. 5, pp. 1126–1139, May 2017.
[15] A. R. Qureshi, M. Acar, S. C. Pires, and L. C. N. de Vreede, "High efficiency and wide bandwidth quasi-load insensitive class-E operation utilizing package integration," *IEEE Trans. Microw. Theory Techn.*, vol. 66, no. 12, pp. 5310–5321, Dec. 2018.
[16] P. E. de Falco *et al.*, "Load modulation of harmonically tuned amplifiers and application to outphasing systems," *IEEE Trans. Microw. Theory Techn.*, vol. 65, no. 10, pp. 3596–3612, Oct. 2017.
[17] T. Barton and P. de Falco, "Outphasing power amplifiers" in *Radio Frequency and Microwave Power Amplifiers: Efficiency and Linearity Enhancement Techniques*. London, U.K.: Inst. Eng. Tech., vol. 2, 2019, pp. 175–223.
[18] D. J. Shepphard, J. Powell, and S. C. Cripps, "An efficient broadband reconfigurable power amplifier using active load modulation," *IEEE Microw. Wireless Compon. Lett.*, vol. 26, no. 6, pp. 443–445, Jun. 2016.
[19] R. Quaglia, J. Powell, D. Shepphard, P. Tasker, and S. Cripps, "Analysis and characterization of a load modulated balanced amplifier for base-station applications," in *Proc. German Microw. Conf.*, 2018, pp. 1–4.
[20] R. Quaglia and S. Cripps, "A load modulated balanced amplifier for telecom applications," *IEEE Trans. Microw. Theory Techn.*, vol. 66, no. 3, pp. 1328–1338, Mar. 2018.
[21] P. H. Pednekar, E. Berry, and T. W. Barton, "RF-input load modulated balanced amplifier with octave bandwidth," *IEEE Trans. Microw. Theory Techn.*, vol. 65, no. 12, pp. 5181–5191, Dec. 2017.
[22] P. H. Pednekar, W. Hallberg, C. Fager, and T. W. Barton, "Analysis and design of a Doherty-like RF-input load modulated balanced amplifier," *IEEE Trans. Microw. Theory Techn.*, vol. 66, no. 12, pp. 5322–5335, Dec. 2018.
[23] D. J. Shepphard, J. Powell, and S. C. Cripps, "A broadband reconfigurable load modulated balanced amplifier (LMBA)," in *Proc. IEEE Int. Microw. Symp.*, 2017, pp. 947–949.
[24] D. Collins, R. Quaglia, J. Powell, and S. Cripps, "Experimental characterization of a load modulated balanced amplifier with simplified input power splitter," in *Proc. Asia-Pacific Microw. Conf.*, 2018, pp. 461–463.
[25] J. Pang *et al.*, "Analysis and design of highly efficient wideband RF-input sequential load modulated balanced power amplifier," *IEEE Trans. Microw. Theory Techn.*, vol. 68, no. 5, pp. 1741–1753, May 2020.
[26] J. R. Powell, D. J. Shepphard, R. Quaglia, and S. C. Cripps, "A power reconfigurable high-efficiency *X*-band power amplifier MMIC using the load modulated balanced amplifier technique," *IEEE Microw. Wireless Compon. Lett.*, vol. 28, no. 6, pp. 527–529, Jun. 2018.
[27] J. Pang, C. Chu, Y. Li, and A. Zhu, "Broadband RF-input continuous-mode load-modulated balanced power amplifier with input phase adjustment," *IEEE Trans. Microw. Theory Techn.*, vol. 68, no. 10, pp. 4466–4478, Oct. 2020.
[28] K. Vivien, P. de Falco, G. Baudoin, O. Venard, P. Felix, and T. Barton, "Load modulated balanced amplifier designed for AM-PM linearity," in *Proc. IEEE 50th Eur. Microw. Conf.*, 2021, pp. 304–307.
[29] K. Chaudhry, R. Quaglia, and S. Cripps, "A load modulated balanced amplifier with linear gain response and wide high-efficiency output power back-off region," in *Proc. Int. Workshop Integr. Nonlinear Microw. Millimetre-Wave Circuits*, 2020, pp. 1–3.
[30] D. J. Collins, R. Quaglia, J. R. Powell, and S. C. Cripps, "The orthogonal LMBA: A novel RFPA architecture with broadband reconfigurability," *IEEE Microw. Wireless Compon. Lett.*, vol. 30, no. 9, pp. 888–891, Sep. 2020.
[31] Y. Cao, H. Lyu, and K. Chen, "Load modulated balanced amplifier with reconfigurable phase control for extended dynamic range," in *Proc. IEEE Int. Microw. Symp.*, 2019, pp. 1335–1338.
[32] L. C. Nunes, P. M. Cabral, and J. C. Pedro, "Study of the GaN HEMT Doherty power amplifier distortion," in *Proc. Int. Workshop Integr. Nonlinear Microw. Millimetre-Wave Circuits*, 2014, pp. 1–3.
[33] L. Piazzon *et al.*, "Effect of load modulation on phase distortion in Doherty power amplifiers," *IEEE Microw. Wireless Compon. Lett.*, vol. 24, no. 7, pp. 505–507, Jul. 2014.
[34] S. C. Cripps, P. J. Tasker, A. L. Clarke, J. Lees, and J. Benedikt, "On the continuity of high efficiency modes in linear RF power amplifiers," *IEEE Microw. Wireless Compon. Lett.*, vol. 19, no. 10, pp. 665–667, Oct. 2009.
[35] G. Collinson and C. Suckling, "Effects of harmonic terminations on power and efficiency of GaAs HBT power amplifiers at 900 MHz," in *Proc. IEE Colloq. Solid-State Power Amplifiers*, 1991, pp. 12/1–12/5.
[36] T. Nojima and S. Nishiki, "High efficiency microwave harmonic reaction amplifier," in *Proc. IEEE Int. Microw. Symp.*, vol. 2, 1988, pp. 1007–1010.
[37] J. Staudinger and G. Norris, "The effect of harmonic load terminations on RF power amplifier linearity for sinusoidal and pi//4 DQPSK stimuli," in *IEEE Symp. Technol. Wireless Appl. Dig.*, 1997, pp. 23–28.
[38] E. Guillena, W. Li, P. L. Gilabert, and G. Montoro, "Prediction of the optimal phase shift between control signals in dual-input power amplifiers," in *Proc. Int. Workshop Integr. Nonlinear Microw. Millimetre-Wave Circuits*, 2020, pp. 1–3.
[39] R. Sinha and A. De, "Theory on matching network in viewpoint of transmission phase shift," *IEEE Trans. Microw. Theory Techn.*, vol. 64, no. 6, pp. 1704–1716, Jun. 2016.
[40] T. W. Barton, A. S. Jurkov, P. H. Pednekar, and D. J. Perreault, "Multi-way lossless outphasing system based on an all-transmission-line combiner," *IEEE Trans. Microw. Theory Techn.*, vol. 64, no. 4, pp. 1313–1326, Apr. 2016.
[41] P. E. de Falco, J. Birchall, S. B. Smida, K. Morris, K. Mimis, and G. Watkins, "Asymmetrical outphasing: Exploiting conjugate continuous modes of operation," in *Proc. IEEE Topical Conf. RF/Microw. Power Amplifiers Radio Wireless Appl.*, 2017, pp. 18–21.
[42] R. Darraji and F. M. Ghannouchi, "Digital Doherty amplifier with enhanced efficiency and extended range," *IEEE Trans. Microw. Theory Techn.*, vol. 59, no. 11, pp. 2898–2909, Nov. 2011.
[43] C. M. Andersson, D. Gustafsson, J. Chani Cahuana, R. Hellberg, and C. Fager, "A 1-3-GHz digitally controlled dual-RF input power-amplifier design based on a Doherty-outphasing continuum analysis," *IEEE Trans. Microw. Theory Techn.*, vol. 61, no. 10, pp. 3743–3752, Oct. 2013.
[44] A. Piacibello, R. Quaglia, V. Camarchia, C. Ramella, and M. Pirola, "Dual-input driving strategies for performance enhancement of a Doherty power amplifier," in *Proc. IEEE Int. Wireless Symp.*, 2018, pp. 1–4.

KIMON VIVIEN (Member, IEEE) received the B.Sc. degree in electrical engineering and the M.Sc. degree in RF system design from the University of Marnes-La-Vallée, France, in 2018, and the Ph.D. degree from Engineering School ESIEE Paris, France, in 2020. In 2019 and 2020, he joined the RF Power and Analog Laboratory, University of Colorado Boulder, Boulder, CO, USA, as an Exchange Student. His research interests include highly efficient and linear power amplifiers.

PAOLO ENRICO DE FALCO (Member, IEEE) received the B.Eng. degree in electronic engineering from the University of Portsmouth, Portsmouth, U.K., in 2013, and the Ph.D. degree from the University of Bristol, Bristol, U.K., in 2018, for his contributions to advanced load modulated RF power amplifier architectures. From 2017 to 2019, he was a Full Member of R&D RF Team, Toshiba Research Europe. From 2019 to 2020, he was a Postdoctoral Associate with the University of Colorado Boulder, Boulder, CO, USA, and an Honorary Senior Research Associate with the University of Bristol, Bristol, U.K. He led a team to first place in the 2016 IMS High Efficiency Power Amplifier design competition and won the 2016 European Microwave Week Graduate Challenge. His research interests include high-efficiency power amplifier and automated RF circuit design.

OLIVIER VENARD received the M.Sc. degree in electronics, sensors, and signal processing from Université Paris-Sud, Orsay, France, in 1996. After being involved on network technologies and embedded electronics with the Centre National d'Etude des Telecommunication, Paris, France. He is currently an Associate Professor with ESIEE and a member of ESYCOM - UMR 9007 CNRS Laboratory, Université Paris-Est, France. His research and teaching interests include signal processing algorithms for sensors and digital communications, non-linear signal processing for linearisation, adaptive signal processing, wireless communications, networks protocols, embedded electronics, and IoT.

GENEVIÈVE BAUDOIN received the Graduate Engineering degree from Ecole Nationale Supérieure des Télécommunications, Paris, France, in 1977, and the habilitation for Ph.D. direction (HDR) from the University of Marne La Vallée, Marne La Vallée, France, in 2000. She was a Lecturer with the University of Paris-Ouest, before she joined Philips Research Laboratory, France, as a Research Engineer and worked on ultrasound signal processing for medical applications. She is currently a Professor Emeritus with ESIEE Paris, France. She is a member of ESYCOM Research Laboratory, Université Gustave Eiffel, France. Her research and teaching interests include digital signal processing, wireless communications, wireless transmitter linearization, transceiver architectures and algorithms for wireless communications, and localization systems.

PASCAL PIERRE-CHARLES-FÉLIX received the M.S. degree in radio frequency and microelectronics from the Integration du Materiau au Système (IMS) Bordeaux, France, in 1998. In 1999, he joined Alcatel MIETEC, as an Analog RF Designer working on transceiver for mobiles phones. In 2003, he joined ST Microelectronics, as an Analog Designer for wireless and Power management circuit for mobiles phones. He is currently a RF-Analog Designer and Project Manager as Somos semiconductor with Marly-Le-Roi, France.

TAYLOR BARTON (Senior Member, IEEE) received the Sc.B., M.Eng., E.E., and Sc.D. degrees from the Massachusetts Institute of Technology, Cambridge, MA, USA. In 2016, she joined the Department of Electrical, Computer, and Energy Engineering, University of Colorado Boulder (CU Boulder), Boulder, CO, USA, where she is currently an Associate Professor and holds the Lockheed Martin Faculty Fellowship. Prior to joining CU Boulder, she was a Postdoctoral Associate with MIT Microsystems Technology Laboratories and then an Assistant Professor with the University of Texas at Dallas, Richardson, TX, USA.

Prof. Barton was the recipient of the AFOSR Young Investigator Award and the NSF CAREER Award.